

Control of Battery Electric Vehicle using Modular Multilevel Converter

Dr. T.Anil Kumar ¹, A.S.Jayanth Varma ²

¹Professor, Department of Electrical and Electronics Engineering, Anurag University, Venkatapur, GhatkesarMedchal- Malkajgiri District, Telangana, India 500088

²PG Student, Department of Electrical and Electronics Engineering, Anurag Group of Institutions (Now Anurag University)

Email: ¹thalluruani@gmail.com, ²asjvarma@gmail.com

Abstract—Energy storage system is significant in (EV) electric vehicles. Several cells are usually connected in series in electric automobiles to improve motor power output voltage. Several electrochemical properties create the charging status (SOC) the difference between cells in battery. This paper refuges energy management and motor drives for electric automobiles using MMC. To adjust the state of the circuit of each battery cell. The following article offers an integrated electronic cell converter with MMC that produce exceptionally low cell discrepancies, without the requirement for traditional circuit balance or a low harmonic output current content. The semi-bridge cell interfaces in this new architecture make battery depletion and recharge very versatile. Included in the converter is a cell balancing control that interacts with cell load on every converter arm. Specific controls can substantially increase the energy usage of the battery depending on how much each cell charges. By utilizing a fuzzy logic controller, the total harmonic distortion may also be minimized. The investigation indicates that, even if the cells are considerably unbalanced, the proposed regulation has no influence on the symmetry of a three-phase voltage.

Index Terms—Electric Vehicles (BEV), Battery, Modular Multilevel Converters (MMC), Fuzzy Logic Controller (FLC), Total Harmonic Distortion (THD), State of Charge (SOC).

I. INTRODUCTION

BATTERY Electric Vehicles (BEV) address an appealing option in contrast to customary vehicles to decreased discharges and natural effects. BEVs, then again, are less modern innovations with significant opportunity to get better away frameworks, particularly for electrical energy [1]. In electric vehicles, the energy stockpiling framework assumes a crucial part. "As a result of its sufficient energy thickness and expenses, lead corrosive or lithium batteries are very popular" [2], [3]. Because of battery low voltage, should be associated in series to accomplish necessary voltage for the driving motor.

Normally, two sorts of adjustment circuits are utilized. "To start with, the squandered energy in equal opposition is utilized to keep up with a similar voltage in all cells." [4]. An energy-moving arrangement of transformers/inductors and converters makes up the second kind of evening out cycle. Energy can be moved from cells with higher terminal pressure or burden conditions to different cells for burden and voltage balance. Despite the fact that interfacing all cells in series infers a similar current, contrasts in cell development spillage flows may bring about an inhomogeneous voltage appropriation and lopsided charge status all through the phone (SOC).

Therefore, certain cells might be totally depleted significantly sooner than others, forestalling the battery pack from being used further. Moreover, because of cell over-burdens or underloads, cell awkwardness can initiate untimely pack breakdown during long cycling. "Therefore, most battery packs contain either inactive or dynamic battery the executives innovations (BMSs)" [4]. Uninvolved BMS, like resistors, release overflow power for more noteworthy SOC cell balance. A progression of foothold drives utilize a regular two-way dc-dc support converter for the battery-based interface bundle. The significant objective is to lessen the quantity of connected series cells. "To improve in general weight and proficiency, a completely fueled battery pack inductor is utilized. Besides, inductor misfortunes, lower functional temperature." [6]

These days, staggered converters are essentially used in medium and high-voltage drives. These issues may be settled with a novel foothold drive design that utilizes particular staggered converters (MMCs) with coordinated electrical cells. The force sources inside the submodules are not equivalent to those found in customary MMCs (SMEs). On account of their low complete consonant mutilation, high cell harmony, and adequacy in yield voltages and flows, MMCs might be

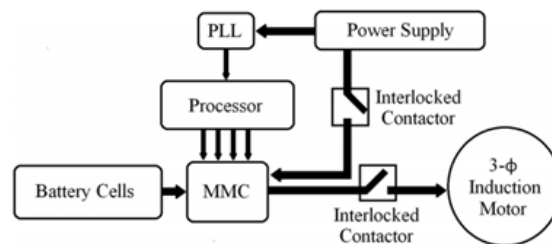


Fig.1 Block Diagram of the System

successfully used in BEV engine drives. Due to the undeniable degree of MMCs and the high recurrence of exchanging, the voltage conveyed by all semi-conductor switches is essentially lower than that of conventional converters. "Measured thoughts may improve the converter's presentation by considering greater adaptability in energy the executives and issue tolerances." [6], [7]

As a deliberately overseen strategy, this examination takes a gander at design of a transformer-dependent on the twofold star, cell adjusting using a group, HB converter, arm, and individual SOC balance regulator. These regulators effectively match the SOC and have the BMS usefulness worked in. Besides, converter can build vehicle accessibility by enduring disappointments in more than one module. "The Fell H-Extension is comprised of two transformer sets that course various H-connect cells into a solitary arm" [9]. When contrasted with the MMC, a fell H-Scaffold by and large has two arrangements of beginning converters. Over the motor, the quantity of MMC modules is multiplied at a similar voltage, however with a large portion of the battery cell limit. Moreover, not at all like CHBs, MMC geographies take into consideration re-energizing from dc, ac, single-stage, or three-

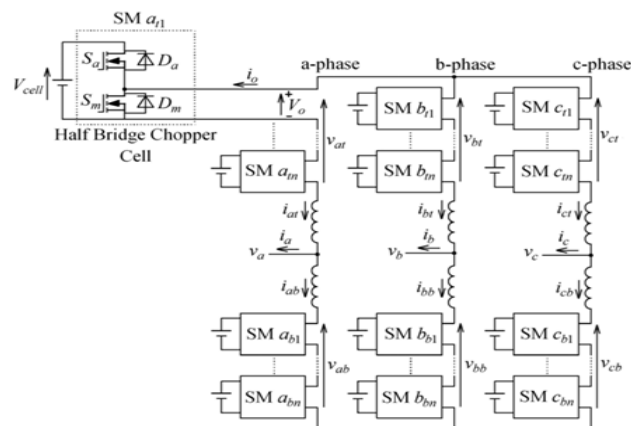


Fig. 2. Electrochemical cells are arranged in the planned MMC's layout.

stage wellsprings of electrochemical cells. "A SPWM transmission module controls the converter, autonomously controlling each MMC stage and evenly creating yield voltages in three phases"[10]. Stage locking circles can be utilized to evaluate recurrence and lattice voltage stages when the converter is associated with an air conditioner power source [10]. With practically a similar force factor stacking the phones, the converter manages the SOC in every one of them.

II. CONVERTER TOPOLOGY

Fig1 illustrates a contour of BEV footing blocks arrangements. MMC is linked with the low engine or the external force supply with the locking button reloading the engine. Figure 2 outlines the planned MMC of solo electrochemical transportation with a semiconductor conversion. Thanks to the voltage level in the SM, MOSFETs may be used as influences switches in order to restrict the converter drive and switch disasters. Rapid enemy of equal exchanging diodes are along these lines forestalled and MOSFET body diodes are delivered uniquely at dead-time crossing points. Two unassembled support inducers interface the converter arms. The stream between the converter legs is limited by a cushion inductor. For a similar explanation, a solitary inductor can likewise be utilised[12], [13].

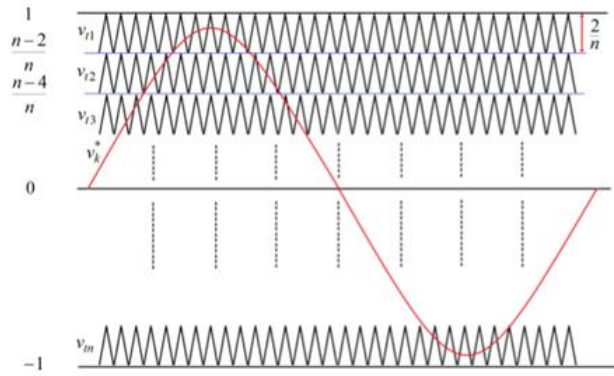


Fig. 3. SPWM Carrier Disposition strategy

This converter is produced by N+1 line-to-fix the AC voltage with n SMs per arm. Voltage is restricted by each exchanging gadget's electric cell voltage.

The functioning standard will be explained for two-way HB chopper cell. Yet in yield voltage is equivalent to V_{cell} , voltage of cell when S_a switch is off. Contingent upon the bearing of current ripple. At point when the Total switch is turned on, the cell's V_0 is 0 furthermore, its SOC stays the same[13]. Each arm's most extreme voltage is $V_{arm,max} = nV_{cell}$, which is the ostensible voltage of the individual cell. Voltage among +ve and -ve transport bar is enhanced by two arms of each leg. The top and $v_{ref, kb}$ are two reference voltages and lower arm of $v_{ref, kt}$.

$$v_{ref, kt} = \frac{V_{arm,max}}{2} - v_k, \quad v_{ref, kb} = \frac{V_{arm,max}}{2} + v_k$$

$$-\frac{V_{arm,max}}{2} \leq v_k \leq \frac{V_{arm,max}}{2} \quad (1)$$

Where v_k is phase voltage and k are the phase, i.e. a, b or c . Thus, $v_{k,max} = \frac{V_{arm,max}}{2}$ is extreme amplitude value of phase voltage.

$$i_{kt} = \frac{i_k}{2} + i_{cir,k}, \quad i_{kb} = -\frac{i_k}{2} + i_{cir,k} \quad (2)$$

As a result of electrochemical cell contrasts, the three legs music happen regardless of whether similar number of SMs is enacted [15], [16]. Simultaneously, round flows can be utilized for cells coursing through the arms. This creates additional misfortune and unbalances without influencing engine flows. In this way, controlling change current is fundamental to boosting cell voltage, which can likewise have different voltages, uncontrolled flows positive equilibrium in productivity and decrease power misfortunes. MMC design is utilized to address the top and base arms of stage K.

$$i_{cir,k} = \frac{i_{kt}}{2} + \frac{i_{kb}}{2} \quad (3)$$

Wherephase upper arm current is i_{kt} is k , phase k lower arm current is i_{kb} , i_k is k Phase current, and $i_{cir,k}$ is current circulating in phase k flows. By solving (2), k flow rate of phase can be expressed as,

$$\begin{aligned} SOC_{h,kt}(t) &= SOC_{h,kt}(t_0) - \frac{1}{3600Q_{max}} \left(\int_{t_0}^t i_{h,kt}(t) dt \right) \\ h &= 1,2,3 \dots, n, \quad k = a,b,c \\ SOC_{h,kb}(t) &= SOC_{h,kb}(t_0) - \frac{1}{3600Q_{max}} \left(\int_{t_0}^t i_{h,kb}(t) dt \right) \\ h &= 1,2,3 \dots, n, \quad k = a,b,c \end{aligned} \quad \text{---- (4)}$$

III. CONTROL STRATEGY OF THE CONVERTER

The converter control consists of two principal segments: the engine control and the SOC. The engine controls are dependent on the usual turning stream vector control and generate three-stage v_k^* voltage references. The PWM modulator [11] is utilized to deliver the MOSFET beats in SMs. This is accomplished by utilizing the sinusoidal Heartbeat Width Regulation. The tweak approach expands on a method to orchestrate transporters with a similar recurrence and plentifulness of n three-sided transporters however with offset for $2/n$ as displayed in Fig3. $V_{k,max}$ is the voltage being standardized. The SOC control for each SM is segregated into a unique adjustment, arm balance and a SOC control group. These restrictions are thoroughly clarified in the surrounding areas. Figure 4 shows the square chart of the SOC-adjusting arm and group.

A. Individual Balancing Control

Without closed loop control, it is the responsibility of the separate balance control to sort and choose active SMs arm for each cell inside the same SOC. The mean for step k top and bottom arm of SOC_{kt} or SOC_{kb} is SOC reference for cells with a similar arm. In an individual SOC adjusting control unit, the dynamic SMs are requested dependent on their rough electrochemical cell SOC [16], [17]. Contingent upon the heading of the stream inside the arm, the arrangement climbs or falls. The dynamic cells with the most elevated fixation level are picked when the current cells are released, and the other way around. Since cells are the peripheral segments of the arm, the need calculation fortifies them to adjust. "The Coulomb tally procedure is utilized to decide the SOC for each cell" [18], [19].

Where the early SOC's are depicted in the top and bottom arms of the cell phase k $SOC_{h,kb}(t_0)$ and $SOC_{h,kt}(t_0)$ respectively, $i_{h,kb}(t)$ and $i_{h,kt}(t)$ are instantaneous currents flowing through h^{th} cell of the top and bottom arms of phase k , and Q_{max} is rated capacity of the cells. SOC estimations can be based on Coulomb counts on their own Because of the inexact findings of cell characteristics, e.g., leakage resistance, interior cell temperature and ageing.

The suggested regulator can take into account the following revision (4):

1) When an electric car fails to operate, the underlying SOC value of t_0 is updated by an estimate of the cell's open-circuit voltage (OCV).

(2) Columbic capability to cover the energy malaises of this regenerative cycle should be increased by the battery current. It relies on the present load and might start from the evaluation [22], [23].

3) The cell potential is a consequence of cell temperature and is predictable [22]. [23].

The currents need not be assessed in Condition (4). It should be seen that current is near in any SM of a comparative arm, as modules are successive associated. Thusly, utilizing an equipped current

$$\begin{aligned} i_{h,kt}(t) &= i_{kt} S_h, & h = 1, 2, \dots, n, & & k = a, b, c \\ i_{h,kb}(t) &= i_{kb} S_h, & h = 1, 2, \dots, n, & & k = a, b, c \end{aligned} \quad (5)$$

$$S_h = \begin{cases} 1, & \text{Top MOSFET is ON} \\ 0, & \text{Top MOSFET is OFF} \end{cases}$$

and a HB converter trading limit, the current stream in each cell can be resolved, and only two current sensors for every leg are required.

A controller is flexible and can be improved to make transformer genuine BEV by adding heatexecutives. For this situation, cell temperatures are controlled for most extreme reach and cell corruption are hence decreased. Cells over as far as possible are thusly excluded and cool off, since they are excluded from the arranging calculation. The cells will be turned around and adjusted when the temperature falls beneath as far as possible in addition to an edge. In the event that the temperature falls beneath chilly restricts, the cells will stay dynamic and warm up until they arrive at a virus limit in addition to a foreordained breaking point. This warm guideline can be expanded considerably further by coordinating stream the executives of the cooling specialist of the cells.

B. Arm Balancing Control

The control of arms balance powers top and base cells in all stage modules to have normal SOC of

$$\left(\frac{\overline{SOC}_{kt}}{\overline{SOC}_{kb}} \right) = \frac{1}{n} \sum_{h=1}^n \left(\frac{SOC_{h,kt}}{SOC_{h,kb}} \right) \quad (6)$$

stage leg. Mean SOCs in stage k is demonstrated in lower arms and upper arms can be displayed as,

At the point when the HB converters disregard their exchanging misfortunes, Immediate influence

$$\begin{aligned} p_{kt} &= v_{kt} i_{kt} = nQ_{max} V_{cell} \frac{d\overline{SOC}_{kt}}{dt} \\ &= \left(\frac{nV_{cell}}{2} - v_k - L \frac{di_{kt}}{dt} \right) i_{kt} \\ p_{kb} &= v_{kb} i_{kb} = nQ_{max} V_{cell} \frac{d\overline{SOC}_{kb}}{dt} \\ &= \left(\frac{nV_{cell}}{2} - v_k - L \frac{di_{kb}}{dt} \right) i_{kb} \end{aligned} \quad (7)$$

can be communicated on top and base arms of the each stage.

Where v_{kb} and v_{kt} are inductance of buffer inductor L in arm voltages. Each phase leg is supplied its differential instantaneous power by

By assume the sinusoidal charge current and voltage are Fourier series Expansion of circulating current

$$\begin{aligned}
 p_{k,diff} &= p_{kt} - p_{kb} \\
 &= nQ_{max}V_{cell} \frac{d(\overline{SOC}_{kt} - \overline{SOC}_{kb})}{dt} \\
 &= \left(\frac{nV_{cell}}{2} - 2v_k - L \frac{di_{kb}}{dt} \right) i_{kb}
 \end{aligned} \tag{8}$$

$$v_k = V_k \sin(\omega t), \quad i_k = I_k \sin(\omega t - \phi) \tag{9}$$

Substituting (9) &(10) in(8), differential power, ignoring alternating terms, are given by

$$p_{k,diff} = nQ_{max}V_{cell} \frac{d(\overline{SOC}_{kt} - \overline{SOC}_{kb})}{dt} \cong -V_k I_{cir,1,k} \cos \theta_1 \tag{11}$$

$$\tag{10}$$

Eq(11) shows that it is effective to balance SOC between upper and lower arms exclusively using fundamental component of circulating current. To make difference SOC_{kt} and SOC_{kb} by proportional controller's output, $I_{cir,1,k}^*$ reference to fundamental component's amplifying range[23].In this paper calculations are accessible so that in highcurrent it may be prevented for design of simpler and

$$\begin{aligned}
 v_{arm,k}^* &= L \frac{d}{dt} [I_{cir,1,k}^* \sin(\omega t + \theta_1)] \\
 &= -\omega L I_{cir,1,k}^* \sin\left(\omega t - \frac{\pi}{2} + \theta_1\right)
 \end{aligned} \tag{12}$$

proportional resonance control.The SOC control's output is $V_{arm,k}^*$, which reflects a voltage drop on buffer inductor due to current's basic element.

Assuming $\phi = \pi/2 - \theta_1$, which is valid at the steady state, (12) becomes.

$$v_{arm,k}^* = -\frac{\omega L}{I_k} I_{cir,1,k}^* i_k = A I_{cir,1,k}^* i_k \tag{13}$$

A block schematic of k-phase arm SOC balancing control is shown in Fig4, whereVoltage control from balance control voltage command $v_{arm,k}^*$ is

Rearranging (11)

$$\frac{d(\overline{SOC}_{kt} - \overline{SOC}_{kb})}{\overline{SOC}_{kt}(s) - \overline{SOC}_{kb}(s)} = \frac{V_k \sin \phi}{BK_3 + As} = BK_3 \tag{16}$$

The arm controller's transfer function is provided by
Which may be used as gainK₃ creation.

C. Cluster Balancing Control

$$v_{arm,k}^* = K_3 (\overline{SOC}_{kt} - \overline{SOC}_{kb}) i_k \tag{14}$$

$$\overline{SOC} = \frac{\overline{SOC}_a + \overline{SOC}_b + \overline{SOC}_c}{3} \quad (17)$$

Average k-phase SOC, \overline{SOC}_k , up to average 3-phase SOC is controlled by cluster balance [19].

$$\begin{pmatrix} \overline{SOC}_a \\ \overline{SOC}_b \\ \overline{SOC}_c \end{pmatrix} = \frac{1}{2n} \sum_{h=1}^n \begin{pmatrix} \overline{SOC}_{h,at} + \overline{SOC}_{h,ab} \\ \overline{SOC}_{h,bt} + \overline{SOC}_{h,bb} \\ \overline{SOC}_{h,ct} + \overline{SOC}_{h,cb} \end{pmatrix} \quad (18)$$

Where

Cluster balance check only the impacts of current component of the fleeting current and does not impact the value of the phased current. dc is derived from the following equation for the general

$$I_{cir,dc,k}^* = K_1(\overline{SOC} - \overline{SOC}_k) \quad (19)$$

phase k circulating current, as shown in Fig. 4.:

$$\begin{aligned} p_{k,total} &= p_{kt} + p_{kb} = 2nQ_{max}V_{cell} \frac{d\overline{SOC}_k}{dt} \\ &= -v_k i_k + nV_{cell} i_{cir,k} - L \left(i_{kt} \frac{di_{kt}}{dt} + i_{kb} \frac{di_{kb}}{dt} \right) \end{aligned} \quad (20)$$

Total instantaneous power of the each phase leg has in Eq(7).

In previous equation alternative term will be disregarded and substituted with (9) & (10) by (20).

Eq(21) it shows how SOC may be balanced by means of current circulating section between 3-legs of a converter[25]. As consequence, $V_{cluster,k}^*$ is given as

$$\begin{aligned} p_{k,total} &= 2nQ_{max}V_{cell} \frac{d\overline{SOC}_k}{dt} \\ &\cong nV_{cell} i_{cir,k} - \frac{1}{2} V_k I_k \cos \phi \end{aligned} \quad (21)$$

$$\begin{aligned} v_{cluster,k}^* &= K_2 (I_{cir,dc,k}^* - I_{cir,dc,k}) \\ &= K_2 [K_1(\overline{SOC} - \overline{SOC}_k) - I_{cir,dc,k}] \end{aligned} \quad (22)$$

$$\overline{SOC}_k(s) = \frac{K_1}{K_1 + 2Q_{max}s} \overline{SOC}(s) - \frac{1}{nV_{cell}} \frac{1}{K_1 + 2Q_{max}s} D(s) \quad (23)$$

If $D(s)$ is $\frac{1}{2} V_k I_k \cos \phi$, cluster controller's closed-loop transfer function is providing by

$$\frac{I_{cir,dc,k}^*(s)}{I_{cir,dc,k}(s)} = \frac{K_2}{K_2 + Ls} \quad (24)$$

Which may be utilized for gaining K1. DC component of circulating current is only if closed loop transfer function.

This may be used to K2 profit model.

Increasing improvements in K1, K2, and K3 will allow the system to more quickly respond to changes and decrease static errors[25]. In order to reduce the output, a larger value is therefore created. The SOC regulates both the cluster and arm by increasing the value of the circulating currents, produces a reference for the converter dc and essential components of the circulating trend voltage. This has saturated both controllers with a voltage level of 5% of the nominal voltage, which lead to a winding effect.

$$\begin{aligned} v_{kt}^* &= v_{cluster,k}^* + v_{arm,k}^* - v_k^* + \frac{nV_{cell}}{2} \\ v_{kb}^* &= v_{cluster,k}^* + v_{arm,k}^* + v_k^* + \frac{nV_{cell}}{2} \end{aligned} \quad (25)$$

The control and control of arm balance is employed to control the reference voltages of the upper and lower arms of phase k.

Fuzzy controller:

In addition, the VOC control system allows use of a dynamic and static internal loop, shown in an outside voltage control loop that allows the picky logical control to adjust DC-link tension at value needed by V {DC}[26]. There are numerous articles in the literature covering a fluffy PWM

$$\begin{aligned} \Delta v_{DC} &= V_{DC}^* - V_{DC} \\ \delta(\Delta v_{DC}) &= \Delta v_{DC}(h) - \Delta v_{DC}(h-1) \end{aligned} \quad (26)$$

corrective device control method. The voltage error and error variation are described as follows in this proposed fuzzy controller:

Controller's output must be discrete modification of d-axis $I_d(h)$ current, in Park domain, in order to progressively increase or decrease reference to existing d-former axis, h1 value is added iteratively:

The inputs of variable bandwidth hysteresis band controller are current phase references[28]. That allows the simplicity and superb undercurrents of hysteretic control to be implemented while

$$I_d(h) = I_d(h-1) + \Delta I_d(h) \quad (27)$$

$$HB = \frac{V_{DC}}{8Lf} \left\{ 1 - \frac{4L^2}{V_{DC}^2} \left[\frac{v_s(t)}{L} - m \right]^2 \right\} \quad (28)$$

maintaining virtually constant switching frequency. As with (28), value of half-bandwidth may be set as:

Where ‘m’is pitch of reference wave's current, V_{DC} is On Dc-link, L is loss of induction in machine and f refers to frequency of switching.

The Half-Bridge converter, once the frequency is selected, transmits gates to maintain the frequency constant at the specified value by adapting the HB to the other system parameters[28].

TABLE I
Circuit Parameters used for Simulations

Load active power	P	65 kW
Load power factor	$\cos\phi$	0.848
Nominal line-line rms voltage	V_n	100 V
Nominal rms current	I_n	442 A
Nominal frequency	f_n	50 Hz
Arm inductor	L	60 Mh
Nominal battery capacity	Q_{max}	20 Ah
Nominal battery voltage	V_{cell}	3.7 V
Control time step	T_s	100 μ s
Number of cells per each arm	n	45
Proportional gain of current controller	K_1	25 A
Proportional gain of cluster controller	K_2	0.5 V/A
Proportional gain of arm controller	K_3	0.04 V

IV. SIMULATION RESULTS

Fig. 5. Comparison of Steady state voltages without and with Fuzzy Logic Controller

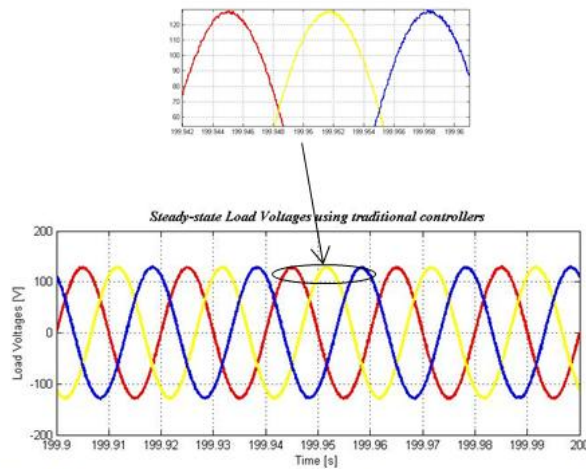


Fig. 5(a). Steady state voltages without using fuzzy logic controller at the output

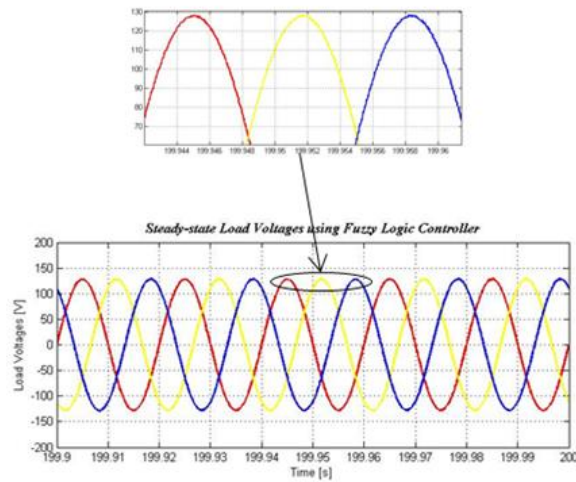
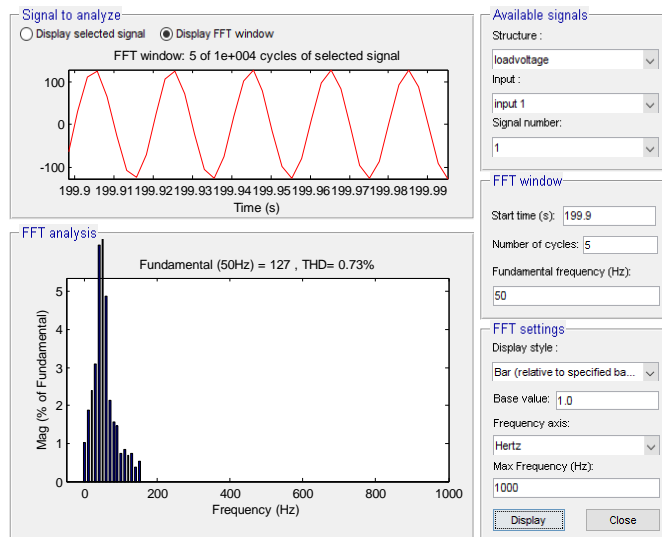
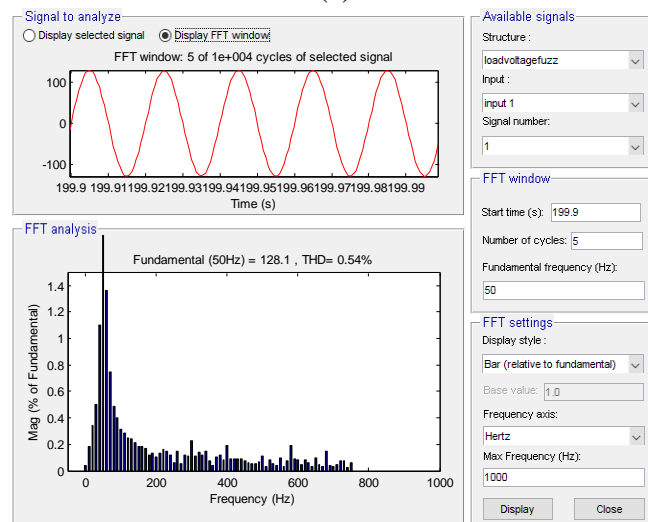


Fig. 5(b). Steady state voltages at the load using fuzzy logic controller



(a)



(b)

Fig 6 Comparison of FFT Analysis without and with FLC. (a) FFT Window of Load Voltage using Traditional Controller.(b) FFT Window of Load Voltage using FLC

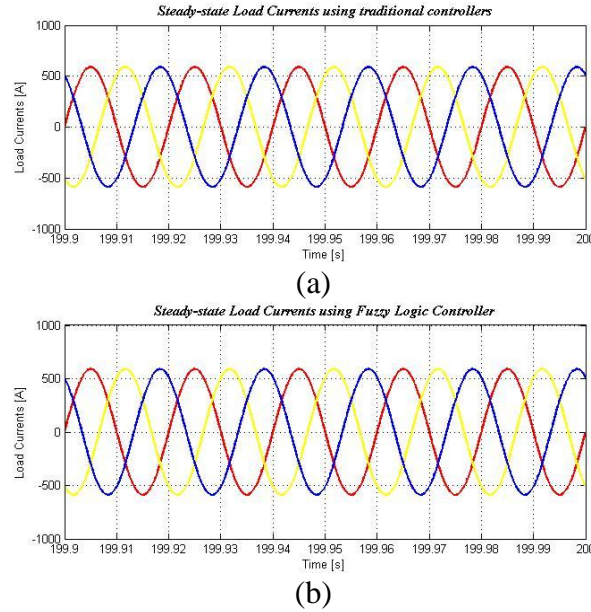


Fig. 7 Comparison of Steady state currents without and with Fuzzy Logic Controller. (a) Steady state currents without using fuzzy logic controller at the output. (b) Steady state currents at the load using fuzzy logic controller.

TABLE II. THD OF LOAD VOLTAGE

NOMINAL INPUT VOLTAGE	% THD IN TRADITIONAL CONTROLLER	% THD BY USING FLC
100 V	0.73	0.54

In this study, numerical simulations were conducted for the operational properties of the proposed MMC with integrated battery cells. Table 1 summarizes the circuit characteristics of the MATLAB / Simulink application and control gains for the simulation. With a maximum imbalance of 15 percent between the more and less charged cells, the initial SOC of the cells was changed.

The converter is made up of 270 Li-ion cells, with 45 cells each arm. 3.7 V is 58V rms and corresponds to 100V line-to-line voltage. The maximum phase voltage of the single cell is 58V rms. A growing number of cells should be utilized to connect greater voltage loads[24] in order to enhance the conversion system efficiency. Furthermore, a higher number of cells would still enhance the harmonical contents of the voltage waveforms.

The battery cells were developed as an ideal voltage source with output voltages which are directly related to their load conditions. The real cell voltages of up and down arms are determined using the

$$\begin{aligned}
 V_{cell_{h,kt}} &= 3 + 1.2SOC_{h,kt} \\
 V_{cell_{h,kb}} &= 3 + 1.2SOC_{h,kb}
 \end{aligned}
 \tag{29}$$

following formulas with a maximum voltage of 4.2 V and a minimum voltage of 3.0 V taken into account:

Each arm is fitted with nominal voltage, the reference voltages of which are normalized, V_{cell} . The reference voltage of the lower arms is 180° behind the reference tension of the upper arms. The number of active module in an arm is estimated by rounding the standard arms reference voltages to

the closest integer[24]. The load voltage and load current are shown in Fig.6 in the cell discharge mode. Because of the load filtering effect, the MMC provides a very low THD (0.54%) and low current deformation.

A formula based on the cell imbalance level is used to measure current circulation (5). The circulating current at the beginning of the simulation is significant as the initial SOC is for the three legs. Like seen in fig. 5, the three circulating currents are not balanced, the controllers of clusters balance cells with circulating currents across the various legs. In a constant state scenario, the cells of each leg are balanced, and the circulatory currents are very little. 5. It is important to note that the charge currents are always balanced, irrespective of the cell condition.

In the first cycle portion, the higher SOC cells are released and the lower SOC cells refilled to some degree identical SOC's in all the cells. The equalization times were compared to the typical active cell balance described under [25] to check the performance of the proposed converter. The suggested converter has been tested for eight Li-ion (4.2 V/10 Ah) batteries per arm with a comparative load of 10 A high inductivity. As shown in [25], cell C1 has the greatest voltage of 4.17 V, cell C2-C7 has the lowest voltage of 3.17 V, cells are 3.67 V.

COMPARISON OF THE PROPOSED MMC WITH DIFFERENT BMSs

Topology	L	C	SW	D	IC	Size	Cost	Equalising Time	Efficiency
SC	0	$n-1$	$2n$	0	0	+	+	±	+++
DTSC	0	n	$2n$	0	0	+	+	++	+++
SSC	0	1	$n+5$	0	0	++	++	+	+++
MSC	0	$n-1$	$2n+2m$	0	0	+	+	+	+++
MSI	$n-1$	0	$2n-2$	0	0	+	+	++	++
SSI	1	0	$2n$	$2n-2$	0	+	+	++	++
SWT	2	0	$n+6$	0	1	+	±	+	+
MWT	$n+1$	0	2	0	1	±	±	+	+
BBC	1	1	$n+7$	0	0	+	+	+++	+++
CC	$2n-2$	$n-1$	$2n-2$	0	0	+	+	++	++
FbC	$2n$	1	$2n$	0	n	±	±	+	+
RC	$n/2$	n	n	n	1	±	±	+	+
MMC	6	0	$2n$	0	0	+	+	+++	+++

L: number of inductors, C: number of capacitors, D: number of diodes, SW: number of switches, IC: number of iron cores, n: number of cells, m: number of SMs. +++ = Excellent, ++ = Very good, + = Good, ± = Satisfactory.

The voltage difference between cells 1 and 8 decreases in 45.93 minutes from 1.0 to 0.5 V compared to the BMS needed in [25], as the balance current can be up to the total load converter power, the proposed circuit is very rapid to equate with the suggested circuit, avoiding constraints on BMS circuits with low power (equal to 6A for the circuit in [25]). In order to fulfil the recharge current and battery cell equalization time necessary, the suggested circulating current converter could be changed. The proposed controller balances all Battery Cells SOC's while keeping the charge voltages and trends constant.

V. OTHER BMSs IN COMPARISON

In comparison with the most popular active BMS topologies, the MMC presented showed its potential for usage with BEVs. The table above compares the different BMSs with respect to the size and cost, time and efficiency of equalization together with the amount of hardware pieces needed for battery cell counts. Capacitor-based solutions offer lower losses of energy compared to inductor/transformer-based and conversion-based procedures. In comparison with the switched condenser (SC), the single switched condenser (SCC), the double level switched condenser (DTSC)

and the modular switched condenser (MSC) method, it is the least energy lost and has adequate equalization times[4].

On the other hand, Multi-Winding Transformer (MWT) and MSI systems will require a short period of time to equal the voltage between the cells, but do not fit Li-ion cells. Furthermore, MWT and MSI have high diameters and a large number of coils and an iron core with considerable magnetic losses. On the other hand, Single Winding (SWT) and Single Winding Inductor (SSI) technology offers rapid equalization time and reduced magnetic losses. The core of SWT must also be modified in order to permit the addition of one or more cells. If SSI demands a high frequency of switching, filter condensers are required. In comparison to Flight Architecture Converter (FbC), CC and Ramper Converters (RC), the buck-boost converter (BBC) technology offers a very quick equalization times with tolerable energy loss[5].

One of the main advantages of the MMC is that although the traction motor is controlled by the same converter, the battery cell balance current is used. Thanks to this, due to added hardware required by standard BMS, cells may be balanced rapidly without further energy waste. The expenses are lowered considerably since the architecture presented avoids high voltage and high-current switches. The hardware design is based on a battery module, resulting, for every half-bridge converter and their controller, in comparatively short lights and control lines. The MMC has the fastest time to equalize, the least power loss and the lowest price and size for any BMS.

VI. CONCLUSION

This study offers a new modular multilevel architecture for BEVs with electrical cells incorporated. To support the conversion structure, a multi-level modular cell half-bridge design with active BMS is employed. According to studies, this design equalizes cells actively and so increases battery life. MMCs with control of the cluster and arm balance are used in this circuit. The suggested study employs the cluster-arm-balancing system Fuzzy Logic Controller to create minimal overall harmonic distortions. This enables the electric car battery pack to replace the balancing circuit with the recommended converters, allowing for the new concept of directly incorporating battery cells into the power converter.

REFERENCES

- [1] J.O. Estima, *et al*, "Efficiency analysis of drive train topologies applied to electric/hybrid vehicles," *IEEE Trans. Veh. Technol.*, vol. 61, no. 3, pp. 1021–1031, Mar. 2012.
- [2] S.D'Arco, *et al*, "A modular converter with embedded battery cell balancing for electric vehicles," in *Proc. Elect. Syst. Aircraft, Railway Ship Propulsion, Bologna, Italy*, Oct. 16–18, 2012, pp. 1–6.
- [3] M.Daowd,*et al*, "Single switched capacitor battery balancing system enhancements," *Energies*, vol. 6, no. 4, pp. 2149–2174, Apr. 2013.
- [4] M.Daowd,*et al*, "Passive and active battery balancing comparison based on MATLAB simulation," in *Proc. IEEE Vehicle Power Propulsion Conf., Chicago, IL, USA*, Sep. 6–9, 2011, pp. 1–7.
- [5] W. Qian, *et al*, "55-kW variable 3X DCDC converter for plug-in hybrid electric vehicles," *IEEE Trans. Power Electron.*, vol. 27, no. 4, pp. 1668–1678, Apr. 2012.
- [6] L. M. Tolbert, *et al*, "Control of cascaded multilevel converters with unequal voltage sources for HEVs," in *Proc. IEEE Int. Electric Mach. Drives Conf., Madison, WI, USA*, Jun. 1–4, 2003, vol. 2, pp. 663–669.
- [7] K. Ilves, *et al*, "On energy storage requirements in modular multilevel converters," *IEEE Trans. Power Electron.*, vol. 29, no. 1, pp. 77–88, Jan. 2014.
- [8] H. Akagi,*et al*, "Classification, terminology, and application of the modular multilevel cascade converter (MMCC)," *IEEE Trans. Power Electron.*, vol. 26, no. 11, pp. 3119–3130, Nov. 2011.

- [9] G. P. Adam, *et al*, "Modular multilevel inverter: pulse width modulation and capacitor balancing technique," *IET Power Electron.*, vol. 3, no. 5, pp. 702–715, Sep. 2010.
- [10] M. Surprenant, *et al*, "Phase tracking locked loop control of inverters in a microgrid," in *Proc. IEEE Energy Convers. Congr. Expo., Phoenix, AZ, USA*, Sep. 17–22, 2011, pp. 667–672.
- [11] G. Ding, *et al*, "An Innovative modular multilevel converter topology and modulation control scheme for the first VSC-HVDC project in China," in *Proc. Power System Comput. Conf., Glasgow, U.K.*, Jul. 14–18, 2008, pp. 1–8.
- [12] Q. Song, *et al*, "A steady-state analysis method for a modular multilevel converter," *IEEE Trans. Power Electron.*, vol. 28, no. 8, pp. 3702–3713, Aug. 2013.
- [13] M. H. Rashid, "Pulse width modulated inverters," in *Power Electronics Circuits, Drives and Applications. 3rd ed.*, Upper Saddle River, USA: Prentice-Hall, 2013.
- [14] X. Yang, *et al*, "Circulating current model of modular multilevel converter," in *Proc. Asia-Pacific Power Energy Eng. Conf.*, Wuhan, China, Mar 25–28, 2011, pp. 1–6.
- [15] Y. Zhang, *et al*, "The control of arm currents and the parameters for modular multilevel converters," in *Proc. 15th Int. Conf. Elect. Mach. Syst., Sapporo, Japan*, Oct. 21–24, 2012, pp. 1–6.
- [16] Z. Li, *et al*, "An inner current suppressing method for modular multilevel converters," *IEEE Trans. Power Electron.*, vol. 28, no. 11, pp. 4873–4879, Nov. 2013.
- [17] A. Lesnicar, *et al*, "An innovative modular multilevel converter topology suitable for a wide power range," in *Proc. IEEE Power Tech Conf., Bologna, Italy*, Jun. 23–26 2003, vol. 3, pp.
- [18] L. Maharjan, *et al*, "State-of-Charge (SOC) balancing control of a battery energy storage system based on a cascade PWM converter," *IEEE Trans. Power Electron.*, vol. 24, no. 6, pp. 1628–1636, Jun. 2009.
- [19] D.J. Deepti, *et al*, "State of charge of lead acid battery," in *Proc. India Int. Conf. Power Electron.*, Chennai, India, Dec. 19–21, 2006, pp. 89–93.
- [20] P. Moss, *et al*, "An electrical circuit for modelling the dynamic response of li-ion polymer batteries," *J. Electrochem. Soc.*, vol. 155, pp. A986–A994, Oct. 2008.
- [21] F. Feng, *et al*, "A combined state of charge estimation method for lithium-ion batteries used in a wide ambient temperature range," *Energies*, vol. 7, pp. 3004–3032, May 2014.
- [22] K. S. Ng, *et al*, "Enhanced coulomb counting method for estimating state-of-charge and state-of-health of lithium-ion batteries," *Appl. Energy*, vol. 86, no. 9, pp. 1506–1511, 2009.
- [23] R. Billinton, *et al*, "Reliability Evaluation of Engineering Systems: Concepts and Techniques", 2nd ed. New York, NY, USA: Plenum Press, 1992.
- [24] S. D'Arco, *et al*, "AC battery charging in modular multilevel converters for electric vehicles," in *Proc. IET Int. Conf. Power Electron., Mach. Drives, Manchester, U.K.*, Apr. 8–10, 2014, pp. 1–6.
- [25] J. Yun, *et al*, "High efficiency active cell balancing circuit with soft switching technique for series-connected battery string," in *Proc. 28th IEEE Appl. Power Electron. Conf. Expo., Long Beach, CA, USA*, Mar. 17–21 2013, pp. 3301–3004.
- [26] Y. Guo, *et al*, "Fuzzy logic based energy storage supervision and control strategy for mvdc power system of all electric ship", *Power and Energy Society General Meeting (PESGM) 2016*, pp. 1-5, 2016.
- [27] M.M.S. Khan, *et al*, "Fuzzy logic based energy storage management system for mvdc power system of all electric ship", *IEEE Transactions on Energy Conversion*, 2017.
- [28] I.J. Cohen, *et al*, Fuzzy logic control of a hybrid energy storage module for naval pulsed power applications, 2016.